

Paper published as:

Tancredi, U.; Renga, A. & Grassi, M. (2011), 'Ionospheric path delay models for spaceborne GPS receivers flying in formation with large baselines', *Advances In Space Research* 48(3), 507--520.

DOI: 10.1016/j.asr.2011.03.04i

Ionospheric path delay models for spaceborne GPS receivers flying in formation with large baselines

Urbano Tancredi^a, Alfredo Renga^b, and Michele Grassi^b

^a*Department for Technologies, University of Naples Parthenope, Centro Direzionale C4, 80143, Italy, urbano.tancredi@uniparthenope.it*

^b*Department of Aerospace Engineering, University of Naples Federico II, Piazzale Tecchio 80, Napoli, 80125, Italy, alfredo.renga@unina.it, michele.grassi@unina.it*

Abstract

This paper focuses on the analysis of ionospheric path delay models for GPS-based relative navigation applications. In particular, the paper aims at assessing if existing ionospheric delay models are suitable for use in real time filtering schemes for the relative navigation of Low Earth Orbit (LEO) satellites flying in formations with large baselines. We specifically refer to real-time filtering schemes, which thus call for relatively simple ionospheric models. We also focus on a navigation scheme that processes double-differenced code and carrier-phase measurements, which, as well known, allow determining the baseline with high accuracy thanks to the possibility of exploiting the integer nature of the double-difference carrier cycle ambiguities. Nevertheless, over large baselines, the success in ambiguity fixing largely depends on the capability of estimating the double-difference ionospheric delays with adequate accuracy. The paper analyzes the capabilities of ionospheric path delay models proposed for spaceborne GPS receivers in predicting both zero-difference and double difference ionospheric delays. Specifically, two models are evaluated, one assuming an isotropic electron density and the other considering the effect on the electron density of the Sun aspect angle. The prediction capability of these models is investigated by comparing predicted ionospheric delay with measured ones on real flight data from the Gravity Recovery and Climate Experiment mission, in which two satellites fly separated of more than 200 km. Results demonstrate that both models exhibit high correlation between predicted and measured ionospheric delays, with the isotropic model performing better than the model including the Sun effect. Moreover, the precision in the estimate is compatible with the use of this model in real-time filtering applications for integer ambiguity fixing.

Keywords: Ionospheric path delays, spaceborne GPS receivers, formation flying, relative navigation, large baseline, double-difference

1 Introduction

Many present and future space missions require the navigation solution to be achieved autonomously on board the satellites. Both absolute and relative navigation are of interest due to the fact that an increasing number of space missions are based on cooperating satellites. For the autonomous navigation of Earth orbiting satellites the GPS plays a crucial role, although some technological and implementation challenges must be faced in order to come to an accurate and robust navigation solution. For instance, the possibility of extracting accurate estimates of the geometric ranges from the GPS observables (code and carrier phase) depends on the capability of properly modeling and predicting some systematic effects, like the ionospheric delay, and estimating biases, like the cycle ambiguities in the carrier-phase observables. In this context, the paper main goal is assessing if existing ionospheric path delay models are suitable for use in real-time filtering schemes for the relative navigation of Low Earth Orbit (LEO) satellites flying in formation with large baselines. Indeed, the differential ionospheric delay caused by the large inter-satellite separation can seriously impact the quality of the relative navigation solution if not properly modeled and predicted.

Formation flying is a topic that is receiving great attention from the international scientific community due to the performance and operational advantages deriving from flying multiple platforms, like increased system flexibility and robustness to failures. Many present and future space missions for Earth remote sensing (Krieger et al. 2007; Moccia and D'Errico, 2008), observation of the universe (Fridlund and Capaccioni, 2002), and Earth gravity field mapping (Tapley et al. 2004) can take advantage from formation flying. In such missions, formation flying requirements can be largely different, with particular concern to the inter-satellite separation and formation navigation and control. We focus on applications that require the satellites to fly at large distances all the time or for a significant fraction of the orbital period, as a result of mission scientific goals. This is the case of remote sensing applications in which parallel or pendulum orbits are considered to reflect next generation monostatic/bistatic spaceborne Synthetic Aperture Radar (SAR) mission needs in LEO. In these applications the baseline can range from a few kilometers to hundreds of kilometers during a single orbit or keep large values during the whole mission (Moccia and D'Errico, 2008; Renga et al. 2008; Renga and Moccia, 2009).

Despite of many performance and operational advantages with respect to traditional space systems, formation flying poses a number of important technology issues, one of which is determining and controlling in real-time the relative positions of the various platforms to maintain or change the formation geometry. Many applications require the determination of the satellite separations with accuracy at the centimeter level to control the satellite relative positions, especially when they come closer

as a result of the relative orbital path, or at the sub-centimeter level to achieve challenging scientific goals (Gill and Runge, 2004; Krieger et al. 2007). Carrier-phase Differential GPS (CDGPS) is a promising technology to implement relative navigation of LEO formations with high accuracy (Busse, 2003; Leung and Montenbruck, 2005). In particular, previous studies show that filtering Double Difference (DD) carrier-phase observables allows determining the satellite relative position with high accuracy, thanks to the possibility of exploiting the integer nature of the related cycle ambiguities (Ebinuma et al. 2003; Leung and Montenbruck, 2005).

A high success rate in fixing the integer ambiguities is crucial to perform the relative navigation with high accuracy. A fundamental contribution to the process of determining the cycle ambiguities is given by the estimation of the DD ionospheric delays. Indeed, DD ionospheric delays scale with the baseline between the receivers, being very small (order of centimeters) only over short baselines (<10 km) (Ebinuma et al. 2003; Leung and Montenbruck, 2005). Over larger baselines (>100 km) they can be higher than several carrier wavelengths, thus seriously impacting the integer ambiguity solution. In presence of large baselines, DD measurements on both frequencies can be exploited to compensate for the DD ionospheric delays. Nevertheless, in order to preserve the integer nature of DD cycle ambiguities, this cannot be achieved by processing the DD measurements by means of ionosphere-free combinations. In addition, ionosphere-free combinations introduce additional noise in the observables, thus affecting the accuracy of the cycle ambiguity fixing process. Therefore, different solutions must be envisaged, such as incorporating in the relative navigation filter suitable ionospheric path delay models. For real-time navigation, such models have to be as simple as possible, while being capable of describing the ionospheric delay with accuracy adequate to the scope, which is fixing the DD integer ambiguities.

In the authors' knowledge, no references can be found in the open literature concerning the use of ionospheric path delay models to predict the DD ionosphere delays for LEO receivers over long baselines. Only a few works report the utilization of ionospheric path delay models in real-time filters for the relative navigation of formation flying satellites. In Ebinuma et al. (2003) and Leung and Montenbruck (2005), the model developed by Lear (1988) is adopted to model the DD ionospheric delay in real-time Extended Kalman Filter applications to formation flying satellites with short inter-satellite separations (<10km), in which single-frequency DD carrier-phase measurements are processed in the filter. Specifically, in Leung and Montenbruck (2005) the filter state vector incorporates a correction term to the nominal vertical delay, whereas in Ebinuma et al. (2003) the vertical ionospheric delay is estimated by the filter, even if it is assumed constant over the baseline due to the short inter-satellite separation. In van Barneveld et al. (2009) two methods for predicting Single Difference (SD) ionospheric delays are reported which can be applied to filtering schemes for the real-time or post-facto relative navigation of satellites with small separations (up to tens of kilometers).

The paper main contribution to the field is assessing the capability of existing ionospheric path delay models to predict DD ionosphere delays with accuracy adequate for use in filters for the relative navigation of LEO receivers. Based on the previous discussion, we specifically refer to LEO satellites flying in formation with large separations and real-time filtering schemes that process DD measurements. The two models of ionosphere path delays developed for LEO receiver applications and described in Lear (1988) are evaluated, based on prediction accuracy requirements complying with the considered relative navigation application. Although primary focus is on DD ionospheric delay prediction, the capability of the two models in predicting the Zero Difference (ZD) ionosphere delays is evaluated as well. Indeed, ZD analysis is instrumental to the interpretation of the results on DD ionospheric delays, and also of potential interest for absolute navigation applications relying on filtering schemes which process data on one frequency (Bock et al. 2009; Psiaki, 2002). Models for ZD and DD ionospheric delay estimate are developed and described in the paper. Finally, the prediction capability of these models is verified by using real flight data from the Gravity Recovery and Climate Experiment (GRACE) mission, launched in 2002.

2 Prediction of ionospheric delays

The effect of the ionosphere on GPS signals is the most important systematic error affecting the GPS signal transmission for LEO receivers. It is well-known that Earth's ionosphere induces a dispersive effect on microwave signals, denoted as ionospheric path delay, and resulting in the phase of the transmitting GPS signal being advanced and in the code transmitted within the GPS signal being delayed. Additional effects (Klobuchar, 1996), such as scintillation and fading, are also present, but are out of the scope of this paper since they are not characterized by systematic and deterministic features.

The availability of dual-frequency GPS signals allows the users to exploit ionosphere-free measurement combinations for substantially cutting down the ionospheric path delay. However, as already outlined in the introduction, in high performance relative positioning and navigation filters, the integer nature of the carrier phase DD ambiguities is exploited to improve the relative navigation accuracy. In this respect, ionosphere-free combinations are challenging since they include a non-integer term involving carrier phase DD ambiguities. When the separations among the satellites are reduced, i.e. for baseline shorter than a few kilometers, the ionospheric contribution to the DD observables is usually on the centimeter scale and therefore it does not affect the integer ambiguity fixing process (Ebinuma et al. 2003; Leung and Montenbruck, 2005). For larger separations (tens to hundreds kilometers) the DD ionospheric delays can be in the order of 30-40 cm or larger, that is, they are larger than the carrier wavelength. In this regard, previous works demonstrate that the relative navigation filter performance is strongly dependent on the baseline, and the filter may diverge for large baselines due to the increasing ionospheric delay error (Bamford, 2004). Different solutions have been therefore envisaged in the open literature to deal with differential ionospheric path delays effects on the integer ambiguity estimation. In Kroes et al. (2005), Kroes and Montenbruck (2004), ionospheric path delays are included in the state vector and for each differential measurement a relevant differential delay is estimated before integer ambiguities are computed. Ionospheric path delays are instead expressed as a function of a reduced number of

parameters that are part of the filter state and are computed before integer ambiguity fixing in Leung and Montenbruck (2005) and Tancredi et al. (2010). In Wolfe et al. (2007) ionospheric path delays are neglected and DD integer ambiguities are derived from wide and narrow lane combinations. The effect of the differential ionospheric path delays are implicitly considered since noise levels about 3 times higher than the actual noise of the measurements have to be used during the ambiguity fixing process, thus resulting in long integer ambiguities estimation times. Each of these solutions has been investigated and proposed as a valid relative navigation scheme for LEO formation flying satellites. However, all these filter structures could benefit notably from an accurate modeling of the ionospheric delays in terms of both speeding up the integer ambiguity estimation process and making it more robust.

2.1 Accuracy requirements

From a quantitative point of view, a proper metric can be introduced to assess if a given ionospheric delay model is suitable for relative navigation. With reference to dual-frequency, double-differenced dynamic (Busse, 2003; Tancredi et al. 2010) and kinematic (Kroes and Montenbruck, 2004) filtering schemes, the usual procedure is to use pseudorange and carrier phase DD measurements simultaneously to estimate a single DD ionospheric delay via a dedicated model. It is expected, therefore, that the measured DD ionospheric delays must be strongly correlated to those predicted by the model. The correlation coefficient is commonly utilized to measure the linear association between two variables. A correlation coefficient greater than 0.8 is usually reckoned to be indicative of strong correlation (Walpole and Myers, 1993), and is considered satisfactory in the remainder of the paper. An additional metric is represented by the root-mean-square (RMS) error of the residuals between the measured and the predicted ionospheric delays, which provides an estimate of the precision in the ionospheric delay prediction. Because the predicted DD ionospheric delays support the integer ambiguity estimation process, a ionospheric delay model can be considered satisfactory if the RMS error is well below the wavelength of the relevant carrier. For instance, under the assumption of normal distribution of the residuals and requiring the three-sigma (3σ) bounds to be within the 19 cm L1 wavelength, it is desirable that the RMS error of the L1 delay prediction is within one sixth of the wavelength, i.e. ~ 3 cm.

The focus of the present investigation is on the prediction of differential ionospheric delays, but, as it will be shown in section 4, the analysis of ZD ionospheric delays, i.e. ionospheric delays affecting the un-differenced GPS observables, is essential to highlight some peculiarities of the DD delay analysis and aids in interpreting the relevant results. For this reason, it is also worth defining accuracy requirements for ionospheric models applied to ZD observables, which are utilized in absolute navigation filtering schemes. For absolute positioning, the filter can take advantage of ionospheric-free combinations if dual-frequency receivers are available. This means that accurate estimates of ZD ionospheric delays may be of interest only for filters processing single-frequency observables. However, most of last generation single-frequency GPS receivers for space applications are characterized by carrier-phase tracking capability, so that GRAPHIC (Group and Phase Ionospheric Corrections) combination of pseudorange and carrier phase observables can be formed to cancel the ZD ionospheric term. This results in observables having the form of biased carrier phase delays (Yunck 1996) with half of the pseudorange noise. A filtering scheme processing GRAPHIC observables has to estimate those biases to produce accurate navigation solutions. If a ionospheric model capable of estimating ZD ionospheric delays with a RMS error lower than that of GRAPHIC observables (10-20 cm) might represent a valid alternative to GRAPHIC combination for absolute navigation, since quite accurate solutions might be generated by a simple filter structure, that does not need to manage biased observables. This topic was investigated in (Bock et al. 2009) where a ionospheric delay model was used based on the Global Ionosphere Map (GIM) delivered by IGS. That model is developed for Earth-based application, thus the predicted delays were reduced accordingly to match the typical LEO ionospheric path delays by means of a constant, empirically determined, scaling factor ranging from 0.3 to 0.4 depending on the receiver altitude. The reported results show that the accuracy of such a model is limited, and therefore GRAPHIC combination should be preferred. The ionospheric models introduced in the following, however, do not rely on GIM data. They have been developed specifically for LEO GPS receivers, but their potential application for single frequency orbit determination in LEO has not been yet investigated. Finally, it is important to point out that, even if marginal, a further application exists that can take advantage of accurate estimations of ZD ionospheric delay. Indeed, single-channel GPS receivers have been proposed (Psiaki, 2002) as a low-power solution for autonomous orbit determination of nanosatellites. In this case 0.5-1 m RMS error in ZD ionospheric delay prediction could be considered satisfactory.

2.2 Selected Models

The first order ZD ionospheric delay in the signal from the GPS satellite i to the receiver A is generally related to the slant Total Electron Content (TEC), i.e. the total electron density along the signal propagation path. For the purposes of the analysis presented in this paper, the inverse-square frequency dependency of the ionospheric delay is deemed adequate, representing first-order ionospheric effects. Higher-order effects are smaller than 1 % of the first-order term at GPS frequencies (sub-millimeter level) and therefore they are neglected in the following (Klobuchar 1996). The ionospheric delay on the L1 frequency, denoted as I , is related to the slant TEC by:

$$I_A^i = \frac{40.3m^3/s^2}{f_1^2} TEC \quad (1)$$

where f_1 is the L1 carrier frequency in Hz and the slant TEC is expressed as the number of electrons per square meter. The superscript refers to the GPS satellite vehicle (SV) transmitting the ranging signal and the subscript to the receiver. Eq. (1) is rarely utilized in navigation filters as it simply transforms the unknown ZD delay in an unknown slant TEC. Models capable

of predicting different ionospheric delays, relevant to different tracked GPS satellites, as a function of a single unknown parameter are instead desirable for navigation filters. A common approach is to linearly relate the different slant TEC to a single Vertical Total Electron Content (VTEC), which depends on time and on the receiver position but not on the observed GPS satellite. Thus, the ionospheric delay can be re-written in terms of the VTEC as:

$$I_A^i = a_A^i \text{VTEC}_A \quad (2)$$

where the linear coefficient a_A^i includes a mapping function, M_i^A , from VTEC to slant TEC, via the formula

$$a_A^i = \frac{40.3 m^3/s^2}{f_1^2} M_i^A \quad (3)$$

DD ionospheric delays can be derived accordingly by linearly combining ZD ionospheric delays (see section 4), thus resulting in a linear model also for the DD delays.

The most used VTEC-based model for LEO receivers is based on the following mapping function proposed by Lear (1988).

$$M_{ISO}(E_A^i) = \frac{2.037}{\sin E_A^i + \sqrt{\sin^2 E_A^i + 0.076}} \quad (4)$$

where E_A^i is the elevation of the GPS satellite i with respect to the receiver A , and the subscript refers to the fact that this mapping function implicitly assumes the electron density to be isotropic. Indeed, it can be shown that Lear's mapping function represents the relationship between the vertical and slant TEC of an ionosphere confined in a shell in whom the electron density is uniform. More precisely, the ionosphere is assumed to be enclosed into a spherical shell of thickness Δh in whom the electron density is uniform both horizontally and vertically. The raypath between the GPS satellite vehicle and the receiver is assumed to be a straight and to fully cross the shell. The latter condition holds because the GPS SV are well above any meaningful maximum ionosphere altitude and the receiver can be assumed to be at an altitude equal to the shell lower bound, since for a LEO receiver the observations are made within the ionosphere and the portion of the ionosphere shell that is below the receiver is unessential. Under these assumptions, the mapping function can be simply expressed as the ratio between the length of the raypath S within the ionosphere and the shell thickness, $M_A^i = S_A^i / \Delta h$. Expressing the length S in terms of the shell thickness and of the SV elevation angle one gets (Spilker, 1996):

$$M_A^i = \frac{2(1 + \Delta\eta/2)}{\sin E_A^i + \sqrt{\sin^2 E_A^i + 2\Delta\eta + \Delta\eta^2}} \quad (5)$$

where $\Delta\eta$ stands for the shell thickness normalized w.r.t. the receiver distance from Earth's center. As such, Lear's isotropic mapping function can be seen as a particular case of the more general isotropic thick shell model. For instance, for a receiver at an altitude of 450 km, Eq.(5) matches Lear's mapping function for $\Delta h \sim 250$ km. Note that, by evaluation of Eq. (5), the variation of h_A and Δh have very limited effects on the values attained by the thick shell mapping function for LEO receivers. Figure 1 compares the thin shell mapping function with the isotropic one for a receiver altitude of 450 km and for reasonable shell thicknesses. Results show that limited differences exist between the two, especially for GPS satellite elevations higher than 10-20 degrees. This suggests that tuning of the shell thickness parameter for the specific application under analysis is of scarce importance, and will not be attempted within this paper.

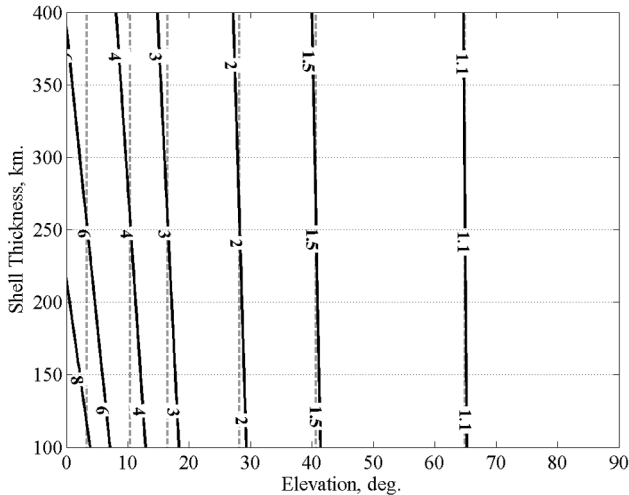


Figure 1. Contour plot of the thick shell mapping function (solid) vs. the isotropic one (dashed) for a receiver altitude of 450 km.

The isotropic mapping function is thus taken as a reference throughout the following analyses. This mapping function is implemented in LEO GPS/GNNS simulators (Leung and Montenbruck, 2005), and ZD ionospheric delays predicted by this model have been demonstrated to be in strong agreement with the results of a rigorous raytracing through a Chapman profile (Garcia-Fernandez and Montenbruck, 2006). However, degraded performance is expected for the isotropic VTEC model at high latitudes, over polar regions, where the ionosphere profile cannot be represented with a Chapman function and important spatial variations of the ionosphere profiles may be observed. The prediction accuracy achieved by the isotropic mapping function has also been assessed for differential ionospheric delays in van Barneveld et al. (2009), but only with reference to single-difference GPS observables and for short baselines (few tens of kilometers). Thus, the evaluation of the mapping function of Eq.(4) in the prediction of DD ionospheric delay and long baselines represents an original contribution of the paper to the field.

In order to overcome some limitations of the isotropic mapping function a different model was proposed by Lear (1988), as well. This mapping function is aimed at including the spatial intensity variation of the ionosphere and the relevant effects on ionospheric delays. The main source of spatial variation of the ionosphere intensity is the night-day cycle. Indeed the atmosphere ionization depends on the Sun position and it is maximum in daylight. For taking into account the average Sun effect, the isotropic mapping function is modified by a multiplying coefficient depending on the local hour

$$M_{SUN} \left(E_A^i, \mathbf{u}_A^i, \mathbf{n}_A \right) = \left[1 + 0.143 \left(\mathbf{u}_A^i \cdot \mathbf{n}_A \right) \right]^8 M_{ISO} \left(E_A^i \right) \quad (6)$$

where \mathbf{n}_A is the unit vector of the equatorial projection of the Sun in the Earth-center Earth-fixed (ECEF) reference frame and \mathbf{u}_A^i is the unit vector pointing towards the i -th GPS satellite vehicle from the receiver A . This model predicts at the local noon ZD ionospheric delays about 3 times higher than the ones at the local dusk or dawn. The average Sun model seems to rely on a more faithful representation of the VTEC spatial variations due to the day-night cycle, so it is expected to perform better than the isotropic one. However, it neglects the delay (of about 2 hours) existing between the maximum of atmosphere ionization and the local noon and uses the equatorial projection of the Sun unit vector, further neglecting the contribution to the atmosphere ionization coming from the actual sun declination. The mapping function corrected for Sun effects is also included in the following analyses. The prediction accuracy of the ionospheric delay model including the average Sun effect has never been investigated with reference to real-world data, and thus represents an additional original contribution of the paper to the field.

Finally, it is worth stressing that the above ionospheric delay models are specifically selected aiming at relative and absolute positioning of LEO satellites. The selected models might not be adequate for a comprehensive analysis of the ionosphere status, but this is not of interest herein. Also note that, due to the geometrical interpretation of the isotropic mapping function, the VTEC estimated by the selected models might not represent the electron content of the vertical column above the receiver. This would be the case if the VTEC distribution around the receiver were not uniform. Instead, the estimated VTEC represents an average value of the actual VTEC distribution in the surroundings of the receiver, weighted by the mapping function.

3 GRACE Data Set Description

The performance of the isotropic and average Sun models is evaluated against actual flight data from spaceborne GPS receivers. According to the previous sections, evaluation of the models is of interest for two receivers flying in formation and

separated by a large baseline, in the order of hundreds of km. Flight data matching these requirements is made available by the Gravity Recovery and Climate Experiment (GRACE) mission, launched in 2002. An overview of the GRACE mission can be found in Tapley et al. (2004). It consists of two identical satellites, GRACE A and GRACE B, in near circular orbits at an initial altitude of approximately 500 km and 89.5 deg. inclination. The satellites are nominally separated from each other by 220 km in the along track direction. The primary mission objective is to map the Earth's gravity field, which is accomplished by the mission's key instruments, the Ka-Band Ranging System (KBR) and high-precision accelerometers. Each spacecraft is also equipped with identical NASA JPL BlackJack GPS receivers (Davis et al. 2000). A post-processed version of GRACE data, known as Level 1B (L1B) data, is made available to the scientific community by JPL's Physical Oceanography Distributed Active Archive Center (PODAAC). The Level 1B data are derived from the processing applied to the raw data described by Wu et al. (2006).

A one-day-long dataset has been selected for the analysis presented in this paper from all available GRACE L1B data. Because GPS receivers' L1B data are available at a sampling rate of 0.1 Hz, this results in more than 8000 samples. The dataset refers to December 1st, 2005, in which GRACE A leads the formation and GRACE B follows at a distance in the order of 202 ± 2.5 km. The orbit altitude ranges between ~450 km and ~490 km during the day, and the mean local time at the ascending node is about 7 AM. GPS L1B data consist of three pseudorange measurements and three carrier phase measurements from code observations on the L1 frequency and semi-codeless tracking on the L1 and L2 frequencies, all at 10-second intervals. As with all GRACE Level 1B data, the time-tags are corrected to GPS time using GPS clock solutions computed in post-processing (Case et al. 2010). A data-editing step has been performed on GPS L1B data, in order to detect and remove outliers in the pseudorange measurements and to discard all observations from GPS satellites whose elevation above the local horizon is smaller than 15 deg. The GRACE GPS measurement noise standard deviation has been found to be smaller for code than for semi-codeless tracking and to be elevation dependant (Kroes, 2006). Representative constant values for the noises standard deviations are 10 cm for pseudorange measurements and 7 mm for carrier phase ones (Tapley et al. 2004).

The KBR data have been also used in the following for validating the integer ambiguities (see section 5). The KBR instrument measures the change in distance between the spacecraft, also known as the biased range, with a precision of 10 μ m. The biased range can be seen as the true range plus an unknown bias. The bias is arbitrary for each piecewise continuous segment of phase change measurements and has to be compensated by a specially designed procedure, described in detail by Kroes (2006). The Level 1B data includes also a GPS Navigation (GNV) data product, which contains an estimate of the two spacecraft Center of Mass (CoM) position and velocity vectors. These estimates are obtained as a product of a precision orbit determination tool (see Wu et al. 2006) and typically have a time-varying accuracy of a few centimeters in position. Both KBR and GNV data allow estimating the baseline between the spacecraft CoM, whereas GPS measurements allow reconstructing the baseline between the two GPS antennas. Therefore, the GPS antenna offset w.r.t. the CoM is compensated when necessary taking into account each spacecraft attitude, which is provided in GRACE L1B data as well.

4 Zero Difference ionospheric delays analysis

The capability of the selected ionospheric delay models in predicting Zero Difference (ZD) delays is evaluated by comparing "measured" ionospheric delays, estimated from GRACE measurements, with "predicted" ionospheric delays, which are those computed by the two models presented in section 2.2. Only pseudorange observables are processed for estimating the measured ZD delays. Even though this approach limits the accuracy of the estimated delays, it is coherent with the objective of evaluating the prediction capability for a filter that does not manage biased observables (as discussed in section 2.1). Given the common structure of the two ionosphere models under analysis, the VTEC for the two GRACE receivers shall be estimated before predicting ZD delays. The procedure for estimating the VTEC profiles, originally proposed in van Barneveld et al. (2008), employs only pseudorange measurements as well. Pseudorange measurements on the L1 and L2 frequencies, P_1 and P_2 , respectively, are modeled by the following equations (Mannucci et al. 1999), which refer only to GRACE A, for brevity.

$$(P_1)_A^i = C_A^i + I_A^i + (b_1)_A + (b_1)^i + (\eta_1)_A \quad (7a)$$

$$(P_2)_A^i = C_A^i + \gamma^{-2} I_A^i + (b_2)_A + (b_2)^i + (\eta_2)_A \quad (7b)$$

Each observable depends on a non-dispersive delay term C , which lumps together the line-of sight geometric distance ρ between the receiver A and the SV i and clock errors, and non-dispersive delays in the hardware signal paths. The L2 ionospheric delay is expressed in terms of I and of the ratio of the two carrier frequencies, $\gamma = f_2 / f_1$. Dispersive receiver and satellite hardware effects are accounted for in the b terms, and the measurement thermal noise is enclosed in the term η . The measured ionospheric delay can be estimated by using the geometry free combination of pseudorange measurements P_1 and P_2 on both GPS frequencies f_1 and f_2 :

$$\hat{I}_A^i = \frac{\gamma}{\gamma^2 - 1} \left[(P_1)_A^i - (P_2)_A^i - b_A - b^i \right] \quad (8)$$

where the dispersive hardware effects are grouped within the receiver and the satellite inter-frequency biases $b_A = (b_1)_A - (b_2)_A$ and $b^i = (b_1)^i - (b_2)^i$, respectively. The combined effect of the two inter-frequency biases might result in a term in the order of several meters (Choi and Glenn Lightsey, 2008). Therefore, their effect has to be compensated for. From inspection of Eq. (7), the geometry-free combination in Eq. (8), compensated for the inter-frequency biases, is an unbiased estimate of the true ionospheric delay (Farrell, 2008), but it has a considerably higher variance than the uncombined measurements. Using GRACE receivers' noise levels, the above estimate of the ionospheric delay has a standard deviation in the order of 30 cm. The satellite vehicle inter-frequency biases are provided as part of the IONEX products by the International GNSS Service (IGS). The receiver inter-frequency biases shall, instead, be estimated from flight data.

The technique for estimating such biases has been originally proposed by van Barneveld et al. (2008), to which we refer the interested reader for the details. It is based on assuming a linear relationship between the ionospheric delay and the VTEC of the receiver, as in Eq.(2). More specifically, by noting that the VTEC is a function only of the receiver position, all ionospheric delays extracted from the n receiver's measurements at each time epoch shall agree with the same VTEC value, on average. Enforcing this condition one can sample the receiver inter-frequency bias for the k -th measurement of the n available as:

$$b_A \approx \left(\frac{1}{n} \sum_{i=1}^n \frac{1}{a_A^i} - \frac{1}{a_A^k} \right)^{-1} \cdot \left(\frac{1}{n} \sum_{i=1}^n \frac{(P_1)_A^i - (P_2)_A^i - b^i}{a_A^i} - \frac{(P_1)_A^k - (P_2)_A^k - b^k}{a_A^k} \right) \quad (9)$$

Receiver inter-frequency biases can be considered as constant over a period of one day (Heise et al. 2005; Sardón and Zarraoa, 1997). This allows having many samples of the bias, and thus estimating it as the mean value by assuming an unbiased samples' distribution. Since each sample's value requires the computation of the linear coefficients of Eq.(2), the inter-frequency biases will be different for the two ionospheric delay models. Table 1 shows the values found using the selected GRACE dataset for the inter-frequency biases, which substantially differ depending on the ionospheric delay model used.

Table 1. GRACE receivers' inter-frequency biases

Ionospheric Delay Model	b_A , m.	b_B , m.
Isotropic	- 6.239	- 4.781
Average Sun	- 6.557	- 5.056

Once the inter-frequency biases have been retrieved and measured delays computed by Eq.(8), the VTEC of each receiver can be estimated at each time epoch by averaging over the visible satellites the values inferred by inverting the ionospheric delay model of Eq.(2). This allows also predicting the delays with the models under consideration. The ZD ionospheric delays predicted by the isotropic and Sun-effect mapping functions are compared with the measured ones in Figures 2, 3. Results demonstrate that delays predicted by the isotropic model are highly correlated with those estimated using GPS measurements. The RMS value is consistent with the variance affecting measured ionospheric delays, suggesting that a substantial fraction of the RMS could be due to the process of extracting ionospheric delays from GRACE measurements rather than to the accuracy of the prediction model. In this perspective, the RMS value of the prediction error can be considered to be a conservative assessment of the model's prediction capability. Nonetheless, the RMS value of the delays prediction error is noteworthy, being a substantial fraction of a meter. Ninety percent of the samples exhibit prediction errors of ± 55 cm at most, being enclosed within the 90th percentile of the prediction error's absolute value distribution (highlighted in dark grey in Figure 2). Considering the 99th percentile, this value increases to about one meter. These results suggest that the isotropic mapping function is not likely to be an alternative to GRAPHIC combinations for absolute navigation by single-frequency code/phase receivers. The attained accuracy, however, could be suitable for single-channel GPS filtering schemes. Including a model of the Sun effect in the ionospheric electron density such as in Eq.(6) does not provide any advantage in predicting the ionospheric delays. On the contrary, the mapping function corrected for Sun effects shows a worse capability of predicting the ionospheric delays, in terms of a 10 % loss in correlation, and, more significantly, of a 90 % increase in the RMS error w.r.t. the isotropic one.

Results point out also a significant limitation of the procedure for computing measured delays. Indeed, the estimated measured delays attain negative values during the day, which is clearly unrealistic. The reason for the negative values of the delays is suspected to be a poor compensation of the receivers' inter-frequency biases. As suggested by Mushini et al. (2009), when the receiver is at higher latitudes (above 60 deg N), there is no proven method for computing an accurate receiver bias, and the estimated bias can be affected by errors that can cause negative estimates of ZD ionospheric delays, as documented in the literature for ground-based receivers (see, e.g., Dyrud et al. 2008). As a consequence of the negative measured ZD ionospheric delays, also the VTEC profile for the receivers attains negative values. The VTEC estimates, shown in Figure 4, exhibit two peaks in each orbit, occurring when the GRACE satellites move near the equatorial bulk of the ionosphere. The VTEC profiles of the two receivers are very similar, except for a slight time delay in the order of tens of seconds, which is consistent with the time necessary for GRACE B to cover the along-track separation distance of ~200 kilometers. When the satellites are above the polar regions, the VTEC attains its minimum (and negative) values, especially in the north pole, since in winter the atmosphere ionization is more intense in the southern hemisphere. These results are in agreement with

previously published VTEC estimates for the GRACE receivers in the same month of December 2005 (van Barneveld et al. 2009). The maximum estimated VTEC value is about 15 TECU (Total Electron Content Unit, corresponding to 10^{16} electrons per square meter) which is well below terrestrial based VTEC levels. This is because the receivers are orbiting at an altitude between 450 and 490 km, which is above a large portion of the ionosphere, and typically above the peak electron density altitude.

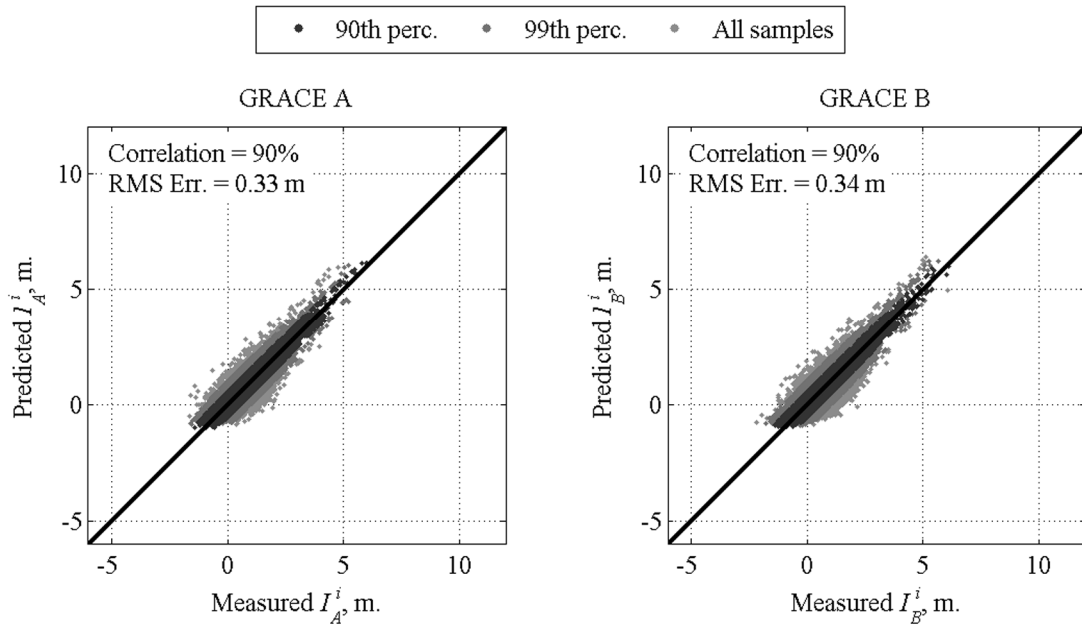


Figure 2. Correlation plot between measured ZD ionospheric delays and those predicted by the isotropic mapping function. Data is colored for enhancing percentiles of the prediction error's absolute value distribution.

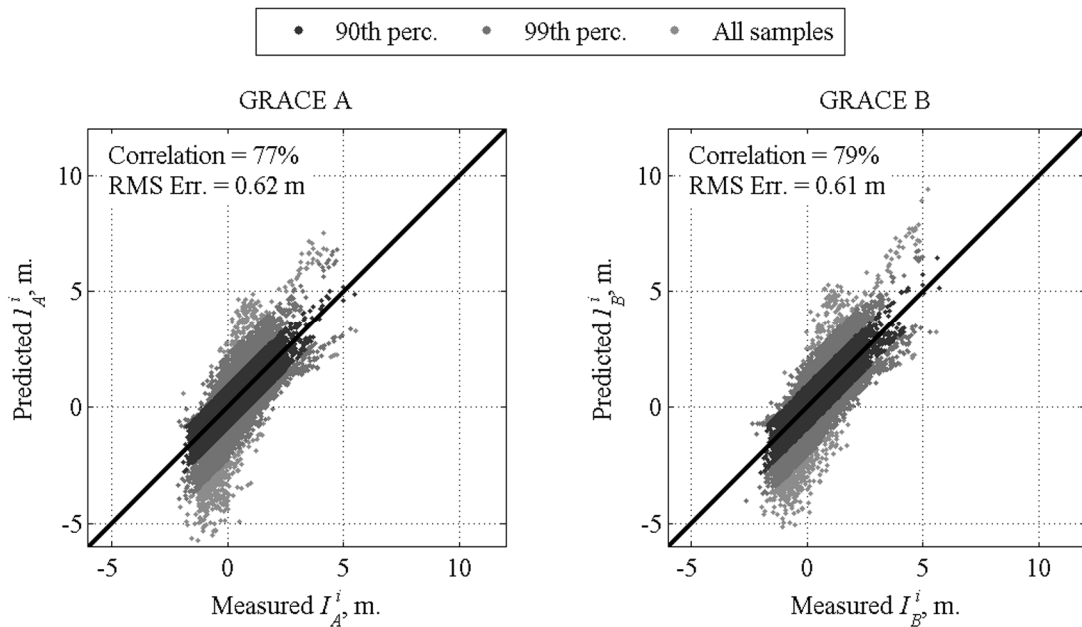


Figure 3. Correlation plot between measured ZD ionospheric delays and those predicted by the Sun-effect mapping function. Data is colored for enhancing percentiles of the prediction error's absolute value distribution.

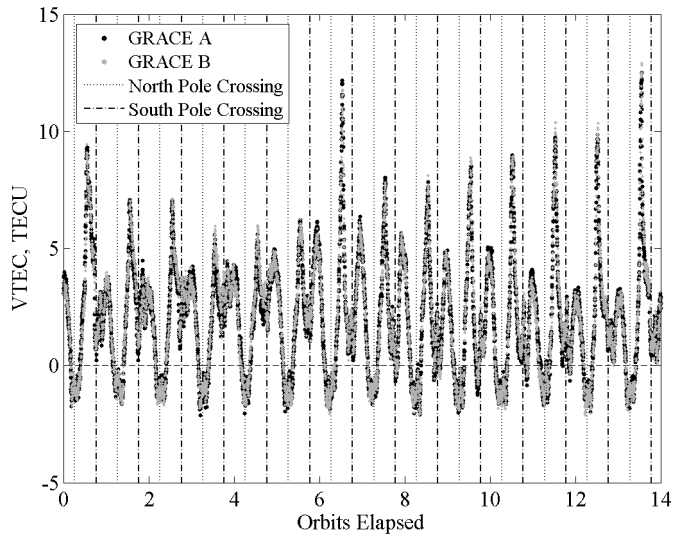


Figure 4. VTEC estimated by the isotropic mapping function.

5 Double Difference ionospheric delays analysis

As previously discussed, prediction of the double difference ionospheric delays is of great importance for relative positioning applications. As for ZD delays, the prediction capabilities of the two ionospheric delay models are evaluated by comparing predicted DD delays with measured ones. Figure 5 shows a schematic of the observation geometry used for computing double differences. SD observations are obtained from ZD ones by taking the difference of measurements from the same GPS satellite vehicle j between the two receivers A and B . Double difference observations are obtained as the difference of the single difference observations between a GPS satellite j , denoted as the pivot, and any other visible satellite k . For simplicity, the pivot is selected as the highest GPS satellite above the horizon. Double difference observations, denoted by a subscript referring to the receivers used in the single difference and by a superscript referring to the couple of GPS satellites used for the double differencing operation, are modeled as:

$$(P_1)_{AB}^{jk} = \rho_{AB}^{jk} + I_{AB}^{jk} + \eta_{1AB}^{jk} \quad (10a)$$

$$(P_2)_{AB}^{jk} = \rho_{AB}^{jk} + \gamma^{-2} I_{AB}^{jk} + \eta_{2AB}^{jk} \quad (8b)$$

$$(L_1)_{AB}^{jk} = \rho_{AB}^{jk} - I_{AB}^{jk} + \lambda_1 (N_1)_{AB}^{jk} + \beta_{1AB}^{jk} \quad (8c)$$

$$(L_2)_{AB}^{jk} = \rho_{AB}^{jk} - \gamma^{-2} I_{AB}^{jk} + \lambda_2 (N_2)_{AB}^{jk} + \beta_{2AB}^{jk} \quad (8d)$$

where L_1 and L_2 refer to ZD carrier phase measurements on the L1 and L2 carrier frequencies, with wavelengths λ_1 and λ_2 , respectively, N stands for the integer carrier cycle ambiguity, and β encloses un-modeled systematic errors on carrier-phase measurements as well as measurement thermal noise. DD observation equations are advantageous over ZD ones thanks to cancellation of most common error terms, such as receiver and satellite biases. The DD ionospheric delay I_{AB}^{jk} is also much smaller than its ZD counterpart, but still significant and larger than the measurement noise when the two receivers are separated by large baselines (tens to hundred kilometers). On the other hand, the differencing operation increases the noise affecting the observation well above the ZD noise level. For instance, in case the noise terms of each ZD observation are considered as uncorrelated zero-mean white noises with same variance, the DD observation noise variance increases of a factor of four. Furthermore, inclusion of the carrier-phase measurements requires estimating and removing the integer ambiguities, and using the same pivot SV j in forming DD observables implies mutual correlation, which shall be carefully considered.

In order to analyze the ionospheric delays, DD observations are compensated for all terms except the ionospheric terms and random noises, yielding the following compensated observations.

$$(P'_1)_{AB}^{jk} = (P_1)_{AB}^{jk} - \rho_{AB}^{jk} \quad (11a)$$

$$(P'_2)_{AB}^{jk} = (P_2)_{AB}^{jk} - \rho_{AB}^{jk} \quad (9b)$$

$$(L'_1)_{AB}^{jk} = (L_1)_{AB}^{jk} - \rho_{AB}^{jk} - \lambda_1 (N_1)_{AB}^{jk} \quad (9c)$$

$$(L'_2)_{AB}^{jk} = (L_2)_{AB}^{jk} - \rho_{AB}^{jk} - \lambda_2 (N_2)_{AB}^{jk} \quad (9d)$$

External data sources are used for compensating the DD geometry term. More precisely, the GRACE GNV Data Product is used for obtaining an estimate of the CoM of each receiver. Such estimate is provided with accuracy in the order of few centimeters. Then, the GPS antenna position is computed for each receiver, by adding the relative offset of the GPS antenna w.r.t. the satellite CoM, taking into account attitude flight data. For computing the ZD line-of-sight geometric ranges, IGS final products are used, which allow estimating the GPS satellite vehicles positions with an accuracy of few centimeters, as well. The DD geometry term is then estimated by the difference of the ZD geometric ranges.

For compensating the carrier cycle ambiguity terms, a standard technique is used for fixing integer ambiguities. The previous estimates of the DD geometric term are used to simplify the integer search procedure. The technique is based (see Goad, 1996) on computing first the wide-lane integer ambiguities, using a weighted least squares solution followed by an exhaustive integer search method. Then, ionospheric-free combinations of DD carrier phase observables are processed in a similar fashion to estimate the integer ambiguities on the L1 and L2 carrier frequencies. This procedure, while being simple and effective thanks to the compensation of the geometry term, does not assure a correct fix of all the integer ambiguities involved in the selected GRACE dataset. Thus, an additional step is performed for validating the computed integer solutions, and eventually discarding the invalid ones. The validation step is based on comparing an estimate of the baseline between the two GRACE receivers obtained by the computed integer ambiguities with an independent accurate estimate of its magnitude, made available by GRACE KBR Data Product. The former estimate builds upon the dependency of the DD geometry term on the baseline, given by:

$$\rho_{AB}^{jk} = \|\mathbf{R}^k - (\mathbf{r}_A + \mathbf{B})\| - \|\mathbf{R}^k - \mathbf{r}_A\| - \|\mathbf{R}^j - (\mathbf{r}_A + \mathbf{B})\| + \|\mathbf{R}^j - \mathbf{r}_A\| \quad (12)$$

where \mathbf{B} is the baseline vector, \mathbf{r}_A is GRACE A position vector, and \mathbf{R}^i stands for the i -th GPS satellite vehicle position vector. Thus, the baseline can be estimated as the Weighted-Least-Square (WLS) solution of ionospheric-free combinations of the DD carrier phase measurements in Eq.(9c,d), compensated for the computed cycle ambiguity terms. The validation step results on the selected dataset suggest that the procedure successfully fixes the ambiguities in 89% of the cases, which implies that 11% of the data samples are discarded. Figure 6 shows the error between the baseline magnitude estimated by KBR data products and the one computed using the validated ambiguities. The RMS error is consistent with the expected accuracy for valid ambiguities, and the lack of jumps in the solution confirms the fixed ambiguities are valid.

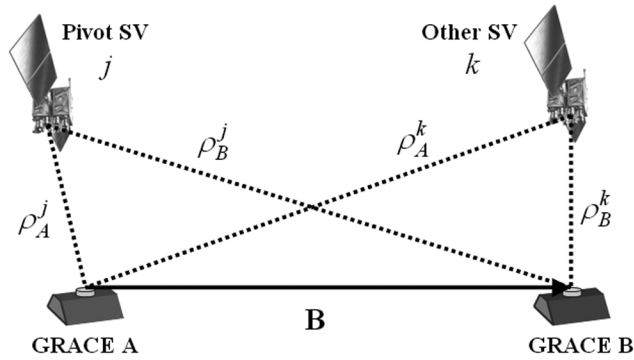


Figure 5. Observation geometry

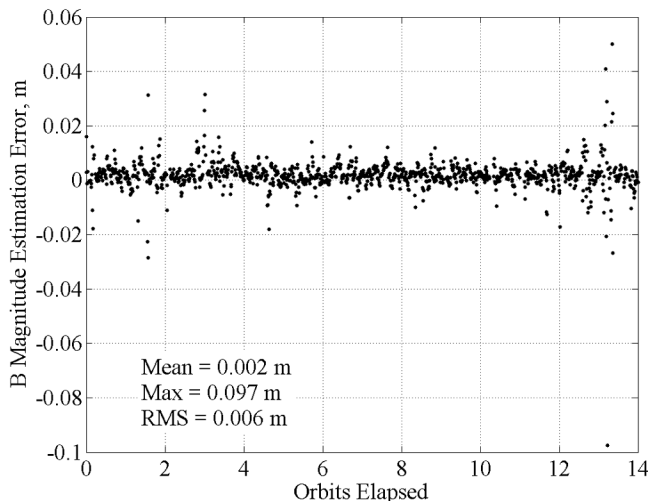


Figure 6. Baseline Magnitude Estimation Error

Measured DD ionospheric delays are obtained taking advantage of geometry and carrier cycle compensation in DD measurements. This approach allows avoiding geometry-free combinations, with related benefits on reducing the noise corrupting the delays estimation procedure, which is particularly desirable when using DD observations. Indeed, due to the double differencing operation, the variance of each measurement increases of a factor of four. On the other hand, for rigorously processing compensated DD measurements, one should take into account the errors introduced by the compensation step. Compensation of the cycle ambiguity terms can contribute, in principle, to the ionospheric delay estimation error. However, the integer nature of the ambiguities implies that effective validation tests can be made on the estimated integer values for identifying and isolating erroneously fixed ambiguities. This allows one to assume meaningfully perfect compensation of the cycle ambiguity terms. The downside of this approach is the appearance in the data of time intervals in which the correct integer ambiguities are not available. In such time intervals, ionospheric delay estimation cannot be attempted. Compensation of the DD geometric term instead introduces an error that can be assumed to be in the order of centimeters. This implies that it can have a non-negligible magnitude with respect to DD carrier phase measurements noise. Nonetheless, modeling this error is not trivial, since it arises because of complex estimation techniques (see, e.g., Wu et al. (2006) for a description of GNV errors). To avoid excessive complication in the estimation procedure, this error term is neglected, and the geometric term is assumed to be perfectly compensated.

In the light of the above remarks, we assume compensated DD measurements to have the same covariance matrix of the uncompensated ones. We assume that the ZD measurements are independent among different receiver-SV couples. However, since DD measurements are obtained by combination of the ZD ones, and the pivot SV j occurs in all measurements at each

time epoch, the DD measurements at a certain time epoch are mutually correlated. In case we have n visible SV, taking $j=1$, denoting generically as X the observation type, i.e. $X = P_1, \dots, L_2$, and as σ_X its standard deviation, the covariance matrix of compensated measurements is as follows.

$$\text{cov} \begin{bmatrix} (X')_{AB}^{12} \\ \dots \\ (X')_{AB}^{ln} \end{bmatrix} = \sigma_X^2 \mathbf{D}, \quad \mathbf{D} := \begin{pmatrix} 4 & 2 & \dots & 2 \\ 2 & \dots & \dots & 2 \\ 2 & 2 & \dots & 4 \end{pmatrix} \quad (13)$$

Exploiting the knowledge of the compensated measurements, at each time epoch the $n-1$ DD ionospheric delays can be estimated using a WLS approach. Let us introduce the following definitions, referring to a single common time epoch, where \mathbf{I} stands for the identity matrix of opportune dimensions:

$$\begin{aligned} \mathbf{x} &:= \left(I_{AB}^{12} \quad \dots \quad I_{AB}^{ln} \right)^T \\ \mathbf{b} &:= \left((P_1)_{AB}^{12} \quad \dots \quad (P_1)_{AB}^{ln} \mid \dots \mid (L_2)_{AB}^{12} \quad \dots \quad (L_2)_{AB}^{ln} \right)^T \\ \text{cov}(\mathbf{b}) = \mathbf{P}_b &:= \begin{pmatrix} \sigma_{P_1}^2 \mathbf{D} & 0 & \dots & 0 \\ 0 & \sigma_{P_2}^2 \mathbf{D} & & \dots \\ \dots & & \sigma_{L_1}^2 \mathbf{D} & 0 \\ 0 & \dots & 0 & \sigma_{L_2}^2 \mathbf{D} \end{pmatrix} \\ \mathbf{A} &:= \left(\mathbf{I} \mid \gamma^{-2} \mathbf{I} \mid -\mathbf{I} \mid -\gamma^{-2} \mathbf{I} \right)^T \end{aligned}$$

An epochwise estimate $\hat{\mathbf{x}}$ of the measured DD ionospheric delays' vector and of its covariance can be obtained as the WLS solution of the linear system obtained by Eq.(10), using the inverse of \mathbf{b} covariance matrix as the weighing matrix.

$$\hat{\mathbf{x}} = \mathbf{P}_x \mathbf{A}^T \mathbf{P}_b^{-1} \mathbf{b} \quad \mathbf{P}_x := \text{cov}(\hat{\mathbf{x}}) = \left(\mathbf{A}^T \mathbf{P}_b^{-1} \mathbf{A} \right)^{-1} \quad (14)$$

Then, for predicting the DD ionospheric delays using Eq.(2), it is necessary to estimate the VTEC profiles over the two receivers. Analogously to the approach used for ZD delays, the VTEC can be estimated by exploiting the estimates available for measured DD delays. In this case, the VTEC estimates can be obtained as the WLS solution of the linear equations (2), using the above estimates. More specifically, let us introduce the epochwise VTEC vector \mathbf{v} and the \mathbf{A}_v matrix as

$$\mathbf{v} := \begin{pmatrix} \text{VTEC}_A \\ \text{VTEC}_B \end{pmatrix}; \quad \mathbf{A}_v = \begin{pmatrix} -(a_A^2 - a_A^1) & (a_B^2 - a_B^1) \\ \dots & \dots \\ -(a_A^n - a_A^1) & (a_B^n - a_B^1) \end{pmatrix} \quad (15)$$

Taking into account the dependency of the measured DD delays covariance matrix in Eq.(14), the estimate of the VTEC above the two receivers is given by:

$$\hat{\mathbf{v}} = \left(\mathbf{A}_v^T \mathbf{A}^T \mathbf{P}_b^{-1} \mathbf{A} \mathbf{A}_v \right)^{-1} \mathbf{A}_v^T \mathbf{A}^T \mathbf{P}_b^{-1} \mathbf{A} \hat{\mathbf{x}} \quad (16)$$

The above equation allows estimating the two VTEC from the $n-1$ measured DD ionospheric delays. On the other hand, there are n equations for estimating each of the two VTEC from ZD measurements. This loss in the number of equations per each unknown clearly results in a noisier estimate of the VTEC from DD measurements when compared to ZD ones. In addition, double differencing the observables increases of a factor of four the noise variance, further worsening the accuracy of the VTEC estimates from DD measurements. As such, it is mandatory to attempt the VTEC estimation exploiting compensated carrier phase measurements. There are time epochs in which the compensated carrier phase measurements are less than the number of visible DD couples, because of the integer ambiguities validation procedure. On the other hand, the number of pseudorange measurements is always equal to the number of visible DD couples. Because of their substantial noise level w.r.t. the magnitude of DD ionospheric delays, DD pseudorange observable alone are of limited usefulness in the present context. We thus choose to discard pseudorange measurements that do not have a carrier phase counterpart. This

implies that measured DD ionospheric delays might not be always available for a visible SV couple jk , depending on the availability of a valid ambiguity solution. Moreover, we also choose to avoid attempting estimation of the two VTEC when less than three measured DD ionospheric delays are available, implying that the VTEC could not be estimated for all time epochs.

The DD ionospheric delays predicted by the isotropic and the Sun effect mapping functions are compared with the measured ones in figures 6, 7. The isotropic mapping function yields predictions of the DD delays that largely correlate with the measured ones. The RMS of the prediction error is in the order of few centimeters, and, as for the ZD case, this is consistent with the variance affecting compensated DD carrier phase observables. More importantly, even this conservative figure for the prediction accuracy is well below the L1 wavelength of 19 cm. By analysis of the prediction error's absolute value distribution, whose 90th and 99th percentiles are shown by color coding in Figures 7,8, it turns out that 97.5 % of the predicted delay are enclosed within the measured ones $\pm \lambda_1/2$, allowing for a correct disambiguation of the carrier cycles. As such, the isotropic mapping function is fit for estimating DD integer ambiguities in a relative positioning filter. As for the ZD delays, the Sun effect correction in the mapping function causes a loss in correlation and degrades the delays prediction accuracy, even though to a less extent. Concerning the VTEC that allows obtaining such performances, results show that completely unrealistic spikes affect the estimated time profiles. The VTEC obtained by Eq.(16) for GRACE A is shown in Figure 9 against the one determined by processing ZD observables. The DD-derived VTEC is seen to be consistent with the ZD one, but much noisier, as expected due to the smaller number of equations and higher noise levels. Nonetheless, there are abrupt oscillations in the VTEC profile when the receiver is above the polar regions. Such huge fluctuations do not cause correspondingly unrealistic DD delays. Indeed, by inspection of Figure 10, it is seen that measured DD delays are reasonable over polar regions, even though they exhibit a qualitatively similar fluctuation. The isotropic mapping function is thus capable of predicting with satisfactory accuracy the measured delays in mid-latitude and equatorial areas. In polar regions, the model still predicts a large part of the fluctuating DD delays, even though with a degraded accuracy. This behavior is consistent with the fact that, as discussed in section 2, the isotropic mapping function is known to work poorly at high latitudes. On the one hand, the unrealistic spikes in the VTEC profile are probably due to the limitations of the model in describing the polar ionosphere, but, on the other hand, are instrumental for reproducing the measured DD delays behavior in the polar regions. We can thus claim that the isotropic model structure still allows to satisfactorily predict the DD delays in these regions, but at the price of an unrealistic VTEC estimation.

The analysis of DD ionospheric delays suggests thus that the two models proposed in section 2 have similar performances. Nonetheless, incorporating the Sun effect in the isotropic mapping function complicates the evaluation of the mapping coefficients a and yields a prediction slightly worse than the un-corrected model. As such, the isotropic mapping function is preferable. By using this model, the DD L1 ionospheric delays between two receivers separated of ~ 200 km can be predicted with an accuracy that is well below the L1 carrier wavelength. This implies that the mapping function can be useful for removing ionosphere delays from un-combined DD carrier phase measurements, and, thus, for streamlining the estimation of the integer ambiguities. For instance, one could include the VTEC of the two receivers in the state of an Extended Kalman Filter, taking advantage of Eq.(2) linearity, as well as of the ease of computation of the mapping coefficients a . Whilst results suggest that the DD delays could be predicted with a satisfactory accuracy, they also point out that the estimated VTEC will not resemble the true one, but it will be characterized by abrupt oscillations and negative values in the polar regions. As such, the VTEC should be modeled within the filter so that the estimate is able to follow such unrealistic dynamics. This could be done, for instance, using a random walk model with a sufficiently large process noise, or, for a more complex model, letting the process noise to be time varying, increasing as the receiver approaches the polar regions.

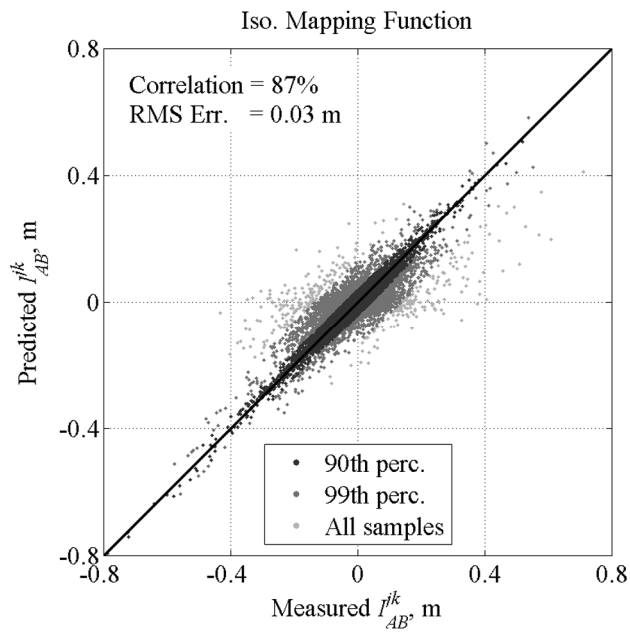


Figure 7. Correlation plot between measured DD ionospheric delays and those predicted by the isotropic mapping function. Data is colored for enhancing percentiles of the prediction error's absolute value distribution.

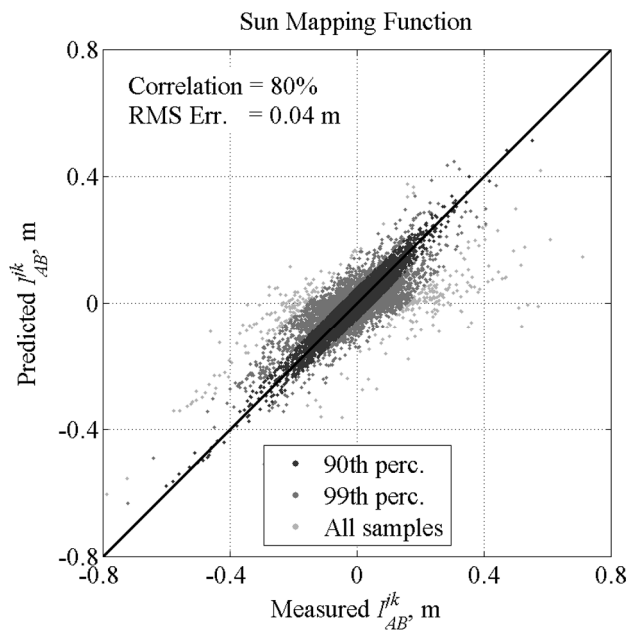


Figure 8. Correlation plot between measured DD ionospheric delays and those predicted by the Sun effect mapping function. Data is colored for enhancing percentiles of the prediction error's absolute value distribution.

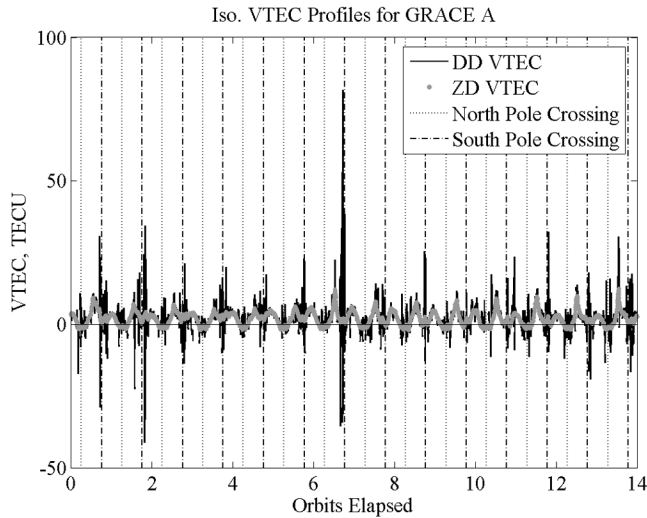


Figure 9. VTEC estimated by the isotropic mapping function from measured DD and ZD ionospheric delays.

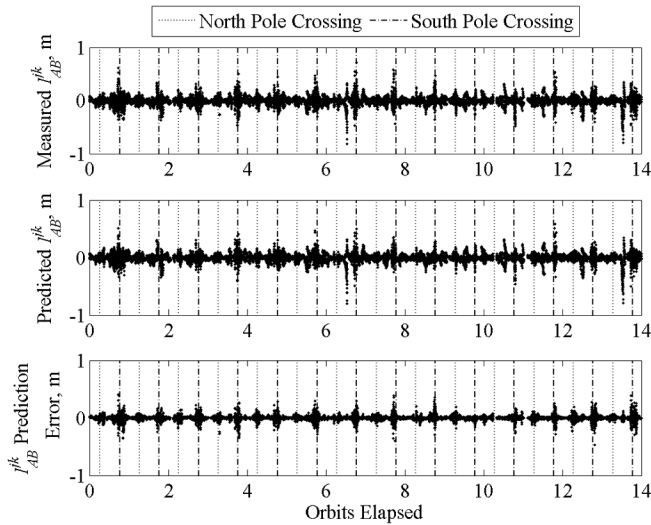


Figure 10. DD ionospheric delays prediction.

6 Conclusion

This paper has investigated existing ionospheric path delay models for spaceborne receivers in terms of their capability of predicting zero difference and double difference ionospheric delays for real-time navigation applications in LEO. Specific attention was given to the prediction of double-differenced ionospheric delays since this is of crucial importance for the relative navigation of LEO satellites flying in formation with large separations. Indeed, in these applications high accuracy in the relative navigation can be achieved by implementing filtering schemes that process double-differenced GPS code and carrier phase observations, in order to exploit the integer nature of the double-difference cycle ambiguities. Nevertheless, the ambiguity fixing process success is strongly influenced by the capability of estimating the double-difference ionospheric delays, which can be of several carrier wavelengths for baselines of hundreds of kilometers. As described in the paper, a mean of predicting these delays with accuracy adequate for the ambiguity fixing is to use a suitable model of the ionospheric path delay. To this end, in the paper two models developed for LEO receiver have been evaluated, one assuming a uniform distribution of the electron density around the receiver (isotropic model), the other considering the effect on this distribution of the Sun aspect angle. Both models have the peculiarity of linearly relating the path delay to the VTEC at the receiver by means of a mapping function, thus being well suited for the implementation into a real-time filter. The test of the prediction performance of these two models on real flight data from the GRACE mission, in which two satellite fly separated of more than 200 km, show that both models are capable of predicting the double-differenced ionospheric delay with accuracy adequate to the considered applications. Nevertheless, the higher correlation between predicted and measured ionospheric delays and precision exhibited by the isotropic model make this last one particularly suited for removing ionospheric delays from DD carrier phase measurements, thus aiding the estimation of the DD integer ambiguities in Extended Kalman filters for relative navigation over large baselines. This could be achieved by augmenting the filter state with the VTEC of each receiver. In this regard, it is worth noting that, as shown in the paper, the VTEC corresponding to the predicted ionospheric delays exhibits an unrealistic behavior, characterized by sudden oscillations and negative values especially in the polar regions, where the adopted models are known to work poorly. Nevertheless, results demonstrate that in these regions the

isotropic model is still capable of predicting the DD ionospheric delays with adequate accuracy, at the price of having an unrealistic VTEC estimation. Therefore, if included in the filter, the VTEC shall be modeled so that its estimate be able to follow such unrealistic dynamics. This could be done, for instance, using a random walk model with a sufficiently large process noise, or letting the process noise to be time varying and increasing as the receiver approaches the polar regions. Finally, the paper shows that the isotropic mapping function exhibits good performance also in the prediction of zero-difference ionospheric delays and the correction for Sun effects worsens the model's performances. However, the isotropic model is not likely to be an alternative to GRAPHIC combinations for absolute navigation by single-frequency code/phase receivers, since it provides a less sharp estimation. The attained accuracy, however, could be suitable for single-channel GPS filtering schemes, which have been proposed as a low-power solution for autonomous orbit determination of nanosatellites.

References

- Bamford, W.A., Jr. Navigation and control of large satellite formations, Ph.D. thesis, The University of Texas at Austin, USA, 2004.
- Bock, H., Jaggi, A., Dach, R., Schaer, S., Beutler G. GPS single-frequency orbit determination for low Earth orbiting satellites, , *Adv. Space Res.* 43, 783–791, 2009.
- Busse, F. D. Precise formation-state estimation in low earth orbit using carrier differential GPS, Ph. D. thesis, Stanford University, 2003.
- Busse, F.D., How, J.P., Simpson, J. Demonstration of adaptive extended Kalman filter for low-earth-orbit formation estimation using CDGPS, *Navigation* 50 (2), 79-93, 2003.
- Case, K., Kruizinga, G., Wu, S.C. GRACE level 1B data product user handbook, NASA Jet Propulsion Laboratory, revision 1.3, JPL D-22027, GRACE 327-733, 2010.
- Choi, K.R., Glenn Lightsey, E. Total electron content (TEC) estimation using GPS measurements onboard TerraSAR-X, in: *Proceedings of the 2008 National Technical Meeting of The Institute of Navigation*, San Diego, pp. 923-935, 2008.
- Davis, G., Davis, E., Luthcke, S., Hawkins, K. Pre-Launch Testing of GPS Receivers for Geodetic Space Missions, in: *Proceedings of the 13th International Technical Meeting of the Satellite Division of The Institute of Navigation*, Salt Lake City, pp. 2009 – 2018, 2000.
- Dyrud, L., Jovancevic, A., Brown, A., et al. Ionospheric measurement with GPS, *Radio Sci.* 43, RS6002, 2008.
- Ebinuma, T., Bishop, R. H., Glenn Lightsey, E. Integrated hardware investigations of precision spacecraft rendezvous using the global positioning system, *J. Guid. Control Dynam.* 26 (3), 425-433, 2003.
- Farrell, J.A. Aided navigation: GPS with high rate sensors, McGraw-Hill, New York, 2008.
- Fridlund, C. V. M., Capaccioni, F. Infrared space interferometry - the DARWIN mission, *Adv. Space Res.* 30 (9), 2135-2145, 2002.
- Garcia-Fernandez, M., Montenbruck, O. Low earth orbit satellite navigation errors and vertical total electron content in single frequency GPS tracking, *Radio Sci.* 41, RS5001, 2006.
- Gill, E., Runge, H. Tight formation flying for an along-track SAR interferometer, *Acta Astronaut.* 55, 473 – 485, 2004.
- Goad, C. Surveying with the global positioning system, in: Parkinson B.W., Spilker, J.J. (Eds.) *Global positioning system: theory and applications*, vol. 2, American Institute of Aeronautics and Astronautics Inc., Washington, pp. 501-517, 1996.
- Heise, S., Stolle, C., Schlüter, S., Jakowski, N. Differential code bias of GPS receivers in low earth orbit: an assessment for CHAMP and SAC-C, in: Reigber, C. Luehr, H., Schwintzer, P., Wickert, J. (Eds.), *Earth Observation with CHAMP—Results from Three Years in Orbit*, Springer, Berlin, pp. 465–470, 2005.
- Klobuchar, J. A. Ionospheric effects on GPS, in: Parkinson B.W., Spilker, J.J. (eds) *Global positioning system: theory and applications*, vol. 1, American Institute of Aeronautics and Astronautics Inc., Washington, pp. 485–515, 1996.
- Krieger, G., Moreira, A., Fiedler, H., et al. TanDEM-X: A satellite formation for high-resolution SAR interferometry, *IEEE Trans. Geosci. Remote Sens.* 45 (11), 3317-3341, 2007.
- Kroes R., Montenbruck O. High accuracy kinematic spacecraft relative positioning using dual-frequency GPS carrier phase data, in: *Proceedings of the 2004 National Technical Meeting of The Institute of Navigation*, San Diego, pp. 607-613, 2004.
- Kroes R., Montenbruck, O., Bertiger, W., Visser, P. Precise GRACE baseline determination using GPS, *GPS Solutions* 9, 21–31, 2005.
- Kroes, R. Precise relative positioning of formation flying spacecraft using GPS, Ph.D. thesis, Delft University of Technology, The Netherlands, 2006.
- Lear W.M. GPS navigation for low-earth orbiting vehicles, NASA Lyndon B. Johnson Space Center, Mission planning and analysis division, 1st revision, NASA 87-FM-2, JSC-32031, 1988.
- Leung S., Montenbruck, O. Real-time navigation of formation-flying spacecraft using global-positioning-system measurements, *J. Guid. Control Dynam.* 28 (2), 226-235, 2005.
- Mannucci, A.J., Iijima, B.A., Lindqwister, U.J., et al. GPS and ionosphere, in: Stone, W.R. (Ed.), *Reviews of Radio Science*, 1996-1999, Oxford Univ. Press, New York, 1999.
- Moccia, A., D'Errico, M. Bistatic SAR for earth observation, in: Cherniakov, M. (Ed.), *Bistatic radar: emerging technology*, John Wiley & Sons Ltd, Chichester, England, 2008.

Mushini, S.C., Jayachandran, P. T., Langley, R. B., MacDougall, J. W. Use of varying shell heights derived from ionosonde data in calculating vertical total electron content (TEC) using GPS - New method, *Adv. Space Res.* 44 (11), 1309-1313, 2009.

Psiaki, M. L. Satellite orbit determination using a single-channel global positioning system receiver, *J. Guid. Control Dynam.* 25 (1), 137-144, 2002.

Renga, A., Moccia, A., D'Errico, M., et al. From the expected scientific applications to the functional specifications, products and performance of the SABRINA mission, in: *Proceedings of the IEEE Radar Conference, Rome*, pp. 1117-1122, 2008.

Renga, A., Moccia, A. Performance of stereo radargrammetric methods applied to spaceborne monostatic-bistatic synthetic aperture radar, *IEEE Trans. Geosci. Remote Sens.* 47 (2), 544-560, 2009.

Sardón, E., Zarraoa, N., Estimation of total electron content using GPS data: How stable are the differential satellite and receiver instrumental biases? *Radio Sci.* 32 (5), 1899-1910, 1997.

Spilker, J.J. GPS Navigation Data, in: Parkinson B.W., Spilker, J.J. (eds), *Global positioning system: theory and applications*, vol. 1, American Institute of Aeronautics and Astronautics Inc., Washington, pp. 121-176, 1996.

Tancredi U., Renga, A., Grassi M. GPS-based relative navigation of LEO formations with varying baselines, in: *Proceedings of the AIAA Guidance Navigation and Control Conference, Toronto, Canada*, 2010.

Tapley, B. D., Bettadpur, S., Watkins, M., Reigber, C. The gravity recovery and climate experiment mission overview and early results, *Geophys. Res. Lett.*, 31, L09607, 2004.

van Barneveld P., Montenbruck O., Visser P. Differential ionospheric effects in GPS based navigation of formation flying spacecraft, in: *Proceedings of the 3rd International Symposium on Formation Flying, Missions and Technology*, ESA/ESTEC, Noordwijk, The Netherlands, 2008.

van Barneveld, P., Montenbruck, O., Visser, P. Epochwise prediction of GPS single differenced ionospheric delays of formation flying spacecraft, *Adv. Space Res.* 44, 987-1001, 2009.

Walpole, R. E., Myers, R. H. *Probability and Statistics for Engineers and Scientists*, 5th Ed., Macmillan Publishing Company, New York, 1993.

Wolfe, J.D., Speyer, J.L., Hwang S., et al. Estimation of relative satellite position using transformed differential carrier-phase GPS measurements, *J. Guid. Control Dynam.* 30 (5), 1217-1222, 2007.

Wu, S.C., Kruizinga, G., Bertiger, W. Algorithm theoretical basis document for GRACE level 1B data processing, NASA Jet Propulsion Laboratory, revision 1.2, JPL D-27672, GRACE 327-741, 2006.

Yunck, T. P. Orbit determination, in: Parkinson B.W., Spilker, J.J. (eds), *Global positioning system: theory and applications*, vol. 2, American Institute of Aeronautics and Astronautics Inc., Washington, pp. 559-592, 1996.